ISSN 1674-1056
http://cpb.iphy.ac.cn
http://iopscience.iop.org/cpb
中国物理 B
Chinese Physics
中国物理 Chinese Physics B

Phosphine-free synthesis of $FeTe_2$ nanoparticles and self-assembly into tree-like nanoarchitectures

Hongyu Wang(王红宇)[1,2], Min Wu(武敏)[1], Yixuan Wang(王艺璇)[1], Hao Wang(王浩)[2], Xiaoli Huang(黄晓丽)[1], Xinyi Yang(杨新一)[1]

Citation: Chin. Phys. B . 2019, 28(10): 106401 . **doi:** 10.1088/1674-1056/ab3b51
Journal homepage: http://cpb.iphy.ac.cn; http://iopscience.iop.org/cpb

What follows is a list of articles you may be interested in

Phase transition of a diblock copolymer and homopolymer hybrid system induced by different properties of nanorods

Xiao-bo Geng(耿晓波), Jun-xing Pan(潘俊星), Jin-jun Zhang(张进军), Min-na Sun(孙敏娜), Jian-yong Cen(岑建勇)
Chin. Phys. B . 2018, 27(5): 058102 . **doi:** 10.1088/1674-1056/27/5/058102

Improving self-assembly quality of colloidal crystal guided by statistical design of experiments

Yizhi Wu(吴以治), Xiaoliang Xu(许小亮), Haiming Zhang(张海明), Ling Liu(刘玲), Jichao Li(李继超), Dabao Yang(杨大宝)
Chin. Phys. B . 2017, 26(3): 038105 . **doi:** 10.1088/1674-1056/26/3/038105

Self-assembly of block copolymers grafted onto a flat substrate: Recent progress in theory and simulations

Zheng Wang(王铮) and Bao-Hui Li(李宝会)
Chin. Phys. B . 2016, 25(1): 016402 . **doi:** 10.1088/1674-1056/25/1/016402

Multiple patterns of diblock copolymer confined in irregular geometries with soft surface

Li Ying, Sun Min-Na, Zhang Jin-Jun, Pan Jun-Xing, Guo Yu-Qi, Wang Bao-Feng, Wu Hai-Shun
Chin. Phys. B . 2015, 24(12): 126403 . **doi:** 10.1088/1674-1056/24/12/126403

Self-assembly of lamella-forming diblock copolymers confined in nanochannels: Effect of confinement geometry

Yu Bin, Deng Jian-Hua, Wang Zheng, Li Bao-Hui, Shi An-Chang
Chin. Phys. B . 2015, 24(4): 046402 . **doi:** 10.1088/1674-1056/24/4/046402

Phosphine-free synthesis of $FeTe_2$ nanoparticles and self-assembly into tree-like nanoarchitectures*

Hongyu Wang(王红宇)[1,2], Min Wu(武敏)[1], Yixuan Wang(王艺璇)[1], Hao Wang(王浩)[2], Xiaoli Huang(黄晓丽)[1,†], and Xinyi Yang(杨新一)[1,‡]

[1] *State Key Laboratory of Superhard Materials, College of Physics, Jilin University, Changchun* 130012, *China*
[2] *College of Material Science and Engineering, Jilin Jianzhu University, Changchun* 130118, *China*

(Received 14 June 2019; revised manuscript received 30 July 2019; published online 30 September 2019)

Manipulating the self-assembly of transition metal telluride nanocrystals (NCs) creates opportunities for exploring new properties and device applications. Iron ditelluride ($FeTe_2$) has recently emerged as a new class of magnetic semiconductor with three-dimensional (3D) magnetic ordering and narrow band gap structure, yet the self-assembly of $FeTe_2$ NCs has not been achieved. Herein, the tree-like $FeTe_2$ nanoarchitectures with orthorhombic crystal structure have been successfully synthesized by hot-injection solvent thermal approach using phosphine-free Te precursor. The morphology, size, and crystal structure have been investigated using transmission electron microscopy (TEM), high-resolution TEM (HRTEM), and powder x-ray diffraction (XRD). We study the formation process of tree-like $FeTe_2$ NCs according to trace the change of the sample morphology with the reaction time. It was found that the $FeTe_2$ nanoparticles show oriented aggregation and self-assembly behavior with the increase of reaction time, which is attributed to size-dependent magnetism properties of the samples. The magnetic interaction is thought to be the driving force of nanoparticle self-organization.

Keywords: self-assembly, transition metal tellurides, phosphine-free Te precursor, tree-like nanoarchitectures

PACS: 64.75.Yz, 81.07.–b **DOI:** 10.1088/1674-1056/ab3b51

1. Introduction

Transition metal telluride (TMT) nanocrystals (NCs) have received significant interest owing to their unique and excellent properties, which offer a wide range of applications in thermoelectrics,[1,2] superconductors,[3] biomedical sciences,[4,5] magnetic semiconductors,[6] and photovoltaics.[7,8] Rational modulation of TMT NCs with a tailored crystal phase, shape, size and/or assembly structure, is of high significance with respect to the engineering of the electronic, optical, and magnetic properties for the design of nanoscale devices with novel functions. Specifically, assembly of uniform nanocrystal building blocks provides a fundamental strategy for the generation of meso- and macroscale nanomaterials.[9,10] Much effort tends to take advantage of NCs as ideal building blocks for the self-assembly into one-dimensional (1D) orderd-array structures, which embody unusual properties and potential uses in both mesoscopic research and the development of nano-devices.[11–14] Many driving forces[15–28] including entropy, ligand–ligand interactions, and magnetic interaction, are contributed to the formation of self-assembly. Recently, magnetic NCs have been widely demonstrated as self-assembly blocks, which depend on the magnetic dipolar interactions of particles of a certain size.[29,30] In this respect, Xu *et al.* used the magnetic dipoles inherently associated with magnetic nanoparticles to form 1D assemblies of NCs.[24] However, the green synthesis and self-assembly of TMT NCs still remain great challenges.

Among of TMTs, iron ditelluride ($FeTe_2$) is an important magnetic semiconductor with narrow band gap, which is known to exhibit 3D magnetic ordering structure. Various $FeTe_2$ nanostructures, such as quantum dots,[31] nanorods,[32,33] and nanosheets,[34] have been prepared by hydrothermal and/or solvothermal method or chemical vapor deposition over the past decade. For instance, Zhang *et al.* reported a hydrothermal route to prepare orthorhombic $FeTe_2$ nanorods in the presence of a certain concentration of KOH.[32] Oyler *et al.* have successfully fabricated $FeTe_2$ nanosheets via a hot-injection route using hexadecylamine, trioctylphosphine oxide, trioctylphosphine, telluride powder, and $[Fe(CO)_5]$.[34] Until now, great endeavors have been devoted to developing facile green synthesis techniques that fabricate TMT NCs. For this purpose, we have recently developed a new strategy for fabricating TMT NCs, *e.g.*, CdTe, PbTe, Cu_2Te, and $FeTe_2$ NCs, by using a highly reactive phosphine-free Te precursor.[31] Despite remarkable synthesis progress in the past decades, the design and construction of the self-assembly $FeTe_2$ NCs have not yet been reported.

In this work, we report on the synthesis of $FeTe_2$ NCs with tunable sizes and their self-assemblies into the tree-

*Project supported by the National Natural Science Foundation of China (Grant No. 11874027) and the China Postdoctoral Science Foundation (Grant Nos. 2019T120233 and 2017M621198).

†Corresponding author. E-mail: huangxiaoli@jlu.edu.cn
‡Corresponding author. E-mail: yangxinyi@jlu.edu.cn

© 2019 Chinese Physical Society and IOP Publishing Ltd

like nanoarchitectures by hot-injection solvothermal method using phosphine-free Te precursor. In this process, we systematically explored the formation process of tree-like $FeTe_2$ nanoarchitectures, and found that the present synthetic process is virtually a combination of oriented aggregation and self-assembly. First, $FeTe_2$ nanoparticles undergo oriented aggregation to form pearl-necklace aggregates. Second, self-assembly process takes place in the shape-defined aggregation, resulting in tree-like $FeTe_2$ aggregates. These $FeTe_2$ nanoparticles display size-dependent paramagnetic–ferromagnetic phase transition at room temperature. This microscopic magnetic behavior affects the macroscopic morphology of the $FeTe_2$, driving the self-assembly of nanoparticles into the tree-like nanoarchitectures.

2. Experimental section

2.1. Chemical reagent

Anhydrous $FeCl_2$ (in purity 99.99%) and TeO_2 powder (in purity 99%) were purchased from Sigma–Aldrich. Dodecanethiol (DDT, 98%), oleylamine (OLA, 80%) were purchased from Alfa Aesar. Methanol, toluene and acetone were obtained from commercial sources. All chemicals were used without further purification.

2.2. Preparation of OLA–Te precursor

Typically, a mixture of DDT (2.0 mL) and TeO_2 powder (0.2 mmol) was loaded into a 20-mL flask and stirred for 5 min at room temperature. Then, the 2.0-mL OLA solution was injected into the mixture to obtain a black solution under a nitrogen atmosphere.

2.3. Preparation of OLA–Fe precursor

Typically, a mixture of anhydrous $FeCl_2$ powder (0.1 mmol) and OLA (5 mL) was loaded into a 50-mL three-neck flask and heated to 200 °C for 10 min under a nitrogen atmosphere to obtain a clear solution.

2.4. Synthesis of orthorhombic $FeTe_2$ NCs

At the temperature point 200 °C, the OLA–Te precursor was injected into the OLA–Fe precursor. The reaction was allowed to proceed at 200 °C for 60 min. Then, the mixture was cooled to room temperature naturally. The resultant NCs were isolated from the growth solution by precipitation with methanol and excess acetone followed by centrifugation for 3 min at 12000 rpm. Subsequently, the residual samples were redispersed in toluene for characterization.

3. Characterization

The transmission electron microscopy (TEM), high-resolution TEM (HRTEM), high-angle annular dark-field scanning transmission electron microscopy (HAADF-STEM), and elemental mapping images were performed on a JEM-2200FS operating at an acceleration voltage of 200 kV. Composition of the specimens was analyzed with an energy-dispersive x-ray spectroscopy (EDX) was collected from the attachment to the JEM-2200FS. Powder x-ray diffraction (XRD) data were collected on a Bruker D8 diffractometer working with a Cu–Kα target. Magnetic measurements were carried out by a Quantum Design MPMS SQUID VSM magnetometer.

4. Results and discussion

Compared with other metal chalcogens, TMTs are much harder to be synthesized owing to the challenge of the preparation of soluble low-toxicity Te precursor.[35–39] OLA–Te, prepared by dissolving TeO_2 in DDT, is an efficient phosphine-free Te source for the synthesis of metal tellurides NCs in our previous works.[31] Here, we report on a strategy for synthesizing tree-like $FeTe_2$ nanoarchitectures by triggering the self-assembly of nanoparticles, in which the preparation process is divided into two parts: (i) the rapid preparation of soluble phosphine-free Te precursor, (ii) the formation of the solution-based tree-like $FeTe_2$ nanoarchitectures (Fig. 1). As indicated in Fig. 1(a), when OLA was injected into the dispersion of TeO_2 powder and DDT, a second-magnitude redox reaction occurred with color change at room temperature. TeO_2 powder is reduced to the soluble $(OLA)_mTe_n$ complexes, meanwhile, DDT is oxidized to disulfides. Then, we injected the

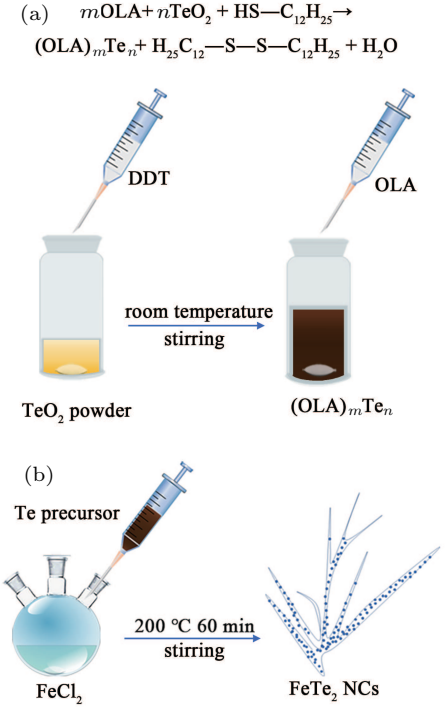


Fig. 1. (a) Schematic diagram for the preparation of the phosphine-free Te precursor and the reaction mechanism. (b) Schematic diagram for the synthesis of $FeTe_2$ NCs obtained at 200 °C, 60 min.

preformed Te precursor into a solution of OLA–Fe precursor to synthesize $FeTe_2$ NCs at 200 °C, 60 min (details see the experimental section).

The morphology of the produced $FeTe_2$ NCs are characterized by transmission electron microscopy (TEM). Figure 2(a) shows a TEM image of the tree-like $FeTe_2$ nanoarchitectures obtained for 60 min, which have many "branches" with the average length in a range of 2 μm–10 μm. We observed the average diameter of the branches were about 40 nm from Fig. 2(b). A higher-magnification TEM image shown in Fig. 2(c) indicates that these tree-like $FeTe_2$ nanoarchitectures consist of a large number of nanoparticles with an average size of 8.8 nm. The as-prepared $FeTe_2$ NCs were examined by XRD at room temperature (25 °C) in Fig. A1 in Appendix A. All diffraction peaks correspond to the crystal structure of $FeTe_2$ with the cell parameter $a = 3.85$ Å (JCPDS File No. 74–0246). The strong diffraction peaks could be indexed to the (101), (110), (111), (012), (020), (121), (200), and (103) planes of orthorhombic $FeTe_2$. The sharp and strong peaks also confirmed that the product is well crystallized. No characteristic peaks for impurities are observed. In addition, the chemical composition of the as obtained product was further checked by EDX (Fig. A2 in Appendix A). The element proportion (atom%) of iron to tellurium is found to be approximately 1:2 as expected (Fe: 35.92%, Te: 64.08%), which is in good agreement with the stoichiometric ratio of the compound of $FeTe_2$. Furthermore, figure 2(d) demonstrates the STEM–EDS mapping images of the tree-like $FeTe_2$ NCs, in which the red region is Te elements, whereas the green region is Fe elements. The result indicates that these elements are uniformly distributed. Therefore, XRD, TEM, and STEM–EDS mapping analyses show that the pure tree-like $FeTe_2$ NCs are successfully synthesized.

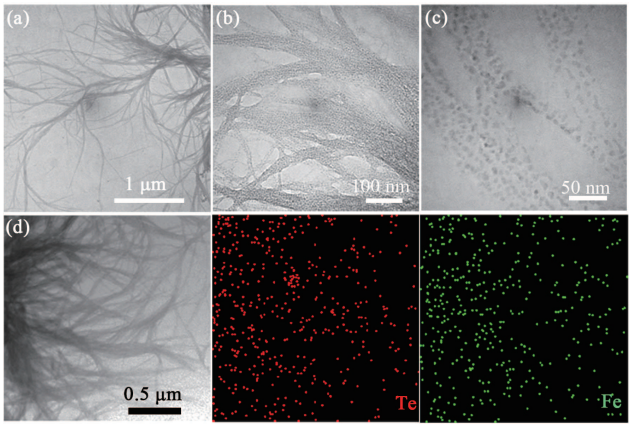


Fig. 2. (a)–(c) TEM images of $FeTe_2$ nanoarchitectures for different magnifications. (d) STEM–EDS mapping of the as-prepared $FeTe_2$ nanoarchitectures.

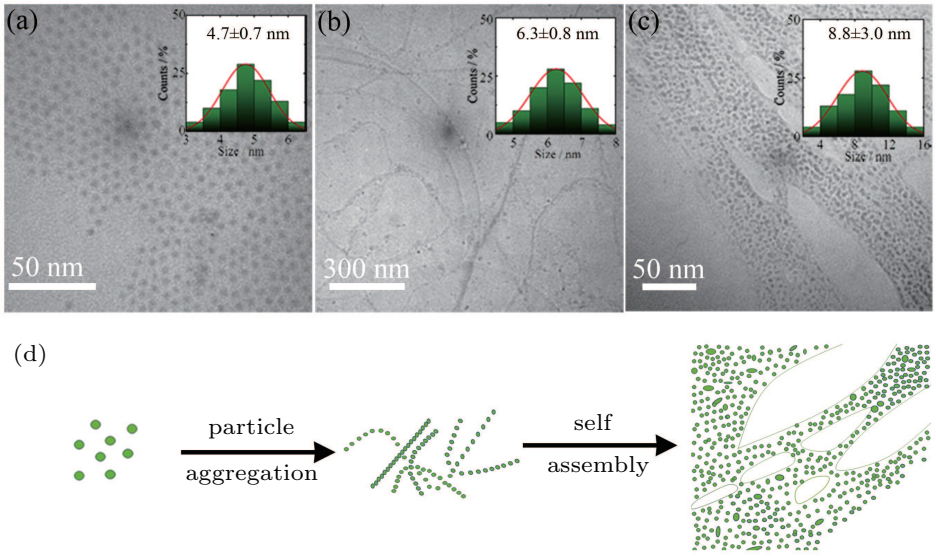


Fig. 3. TEM images of $FeTe_2$ NCs at 200 °C for different reaction time: (a) 10 min, (b) 30 min, and (c) 60 min. The insets show the corresponding size distribution histograms. (d) Schematic diagram for the self-assembly process of the tree-like $FeTe_2$ nanoarchitectures.

In order to study the formation process of tree-like nanostructures, we track the change of sample morphology with the increasing reaction time. Figures 3(a)–3(c) show the TEM images of $FeTe_2$ that are synthesized with the reaction time of 10, 30, and 60 min. In initial, these particles with the size of 4.7 nm were synthesized for 10 min, which have a high degree of monodispersity in Fig. 3(a). The HRTEM image of a single nanoparticles shown in Fig. A3 in Appendix A exhibits that the fringe spacing is about 0.27 nm, corresponding to the (120) plane of orthorhombic $FeTe_2$. When prolonging the reaction time to 30 min, larger $FeTe_2$ nanoparticles about 6.3 nm were produced and spontaneously reorganize to the "pearl-necklace" agglomerates, which have a chain length of 2 μm–10 μm in Fig. 3(b). This result is consistent with the branch length of the tree-like $FeTe_2$ aggregates. With increasing the reaction time to 60 min, the diameters of the as-synthesized $FeTe_2$ nanoparticles increase to 8.8 nm. And nanoparticles of $FeTe_2$ were found to self-assembled into the

tree-like aggregates as shown Fig. 3(c). A schematic illustration of the growth and self-assembly process of the tree-like $FeTe_2$ nanocrystals at different reactions intervals is given in Fig. 3(d).

To further inspect the self-assembly behavior of $FeTe_2$ nanoparticles, we investigated magnetic properties of the samples with different particle sizes. The temperature dependence of magnetization measured in an applied field of 1000 Oe (1 Oe = 79.5775 $A{\cdot}m^{-1}$), clearly sheds light on the magnetic properties of these $FeTe_2$ NCs (Fig. 4). From the zero-field-cooled (ZFC) and field-cooled (FC) curves of 4.7-nm nanoparticles obtained by the reaction time of 10 min, it can be seen that the magnetization measurements show paramagnetic behavior above 75 K (Fig. 4(a)). Therefore, these particles obtained under this condition have good monodispersion. In contrast, the zero-field-cooled (ZFC) and field-cooled (FC) curves of $FeTe_2$ obtained for 60 min are closed until 300 K (Fig. 4(b)), which indicates that the as-prepared tree-like $FeTe_2$ NCs are ferromagnetic at room temperature.

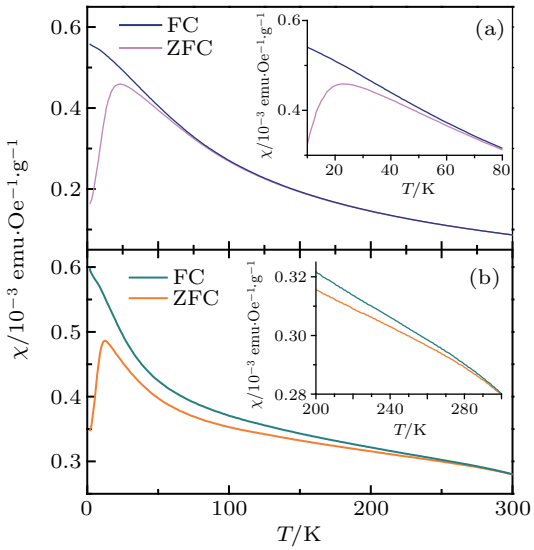


Fig. 4. Temperature dependence of FC and ZFC susceptibilities for (a) 4.7 nm and (b) 8.8 nm $FeTe_2$ NCs.

To gain further insight into the magnetic properties of the synthesized 4.7-nm and 8.8-nm $FeTe_2$ NCs, the magnetization dependence on the applied magnetic field (hysteresis loop) has been recorded at 20 K and 300 K (Fig. 5). The loops indicate that the 4.7-nm and 8.8-nm $FeTe_2$ NCs both have ferromagnetism at 20 K. At 300 K, 4.7-nm $FeTe_2$ NCs show the paramagnetic behavior, whereas 8.8-nm $FeTe_2$ NCs still display ferromagnetic behavior with the coercive force of about 22 Oe. It is in good agreement with the result of the ZFC–FC curves. Thus, we suggest that $FeTe_2$ NCs have the size-dependent magnetic properties. With the increasing reaction time, the diameters of the as-synthesized $FeTe_2$ nanoparticles increase from 4.7 nm to 8.8 nm and spontaneously reorganize to the tree-like aggregates. Therefore, the magnetic interaction is thought to be the driving force of nanoparticle self-organization.

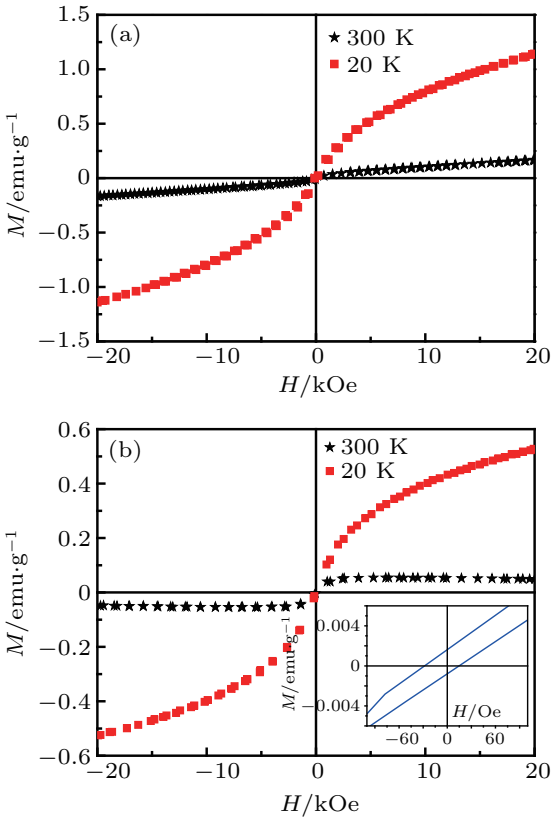


Fig. 5. The hysteresis loop of the synthesized (a) 4.7-nm and (b) 8.8-nm $FeTe_2$ NCs at 20 K and 300 K. The inset of panel (b) is the region around the zero field of the hysteresis loop.

5. Conclusion

In summary, we have proposed a facile way to fabricate $FeTe_2$ NCs using highly reactive phosphine-free Te precursor by hot-injection solvent thermal method. We systematically explored and found that the formation process of tree-like $FeTe_2$ nanoarchitectures is a combination of oriented aggregation and self-assembly. Initially, the $FeTe_2$ nanoparticles with a high degree of monodispersity are formed after nucleation. Subsequently, the $FeTe_2$ nanoparticles undergo oriented aggregation to form the "pearl-necklace" agglomerates. Then, these "pearl-necklace" agglomerates spontaneously assemble into the tree-like nanoarchitectures. The magnetization measurements show the size-dependent magnetic properties of $FeTe_2$ NCs, driving the self-assembly of nanoparticles into the tree-like aggregates. This work provides a simple green approach to integrate $FeTe_2$ NCs with self-assembly behavior, which is suitable for subsequent processing into quantum-confined superstructures, materials, and devices.

Appendix A: Supporting information

Some figures are given in the following to provide supporting information for better understanding the text.

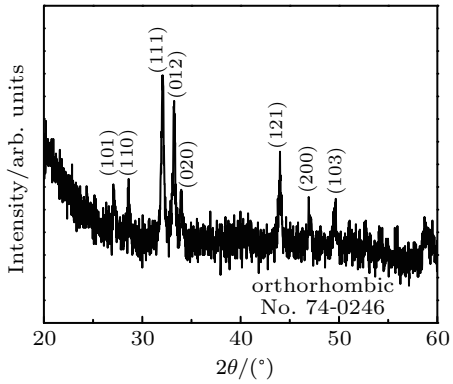


Fig. A1. XRD characterization of orthorhombic $FeTe_2$ prepared for 60 min.

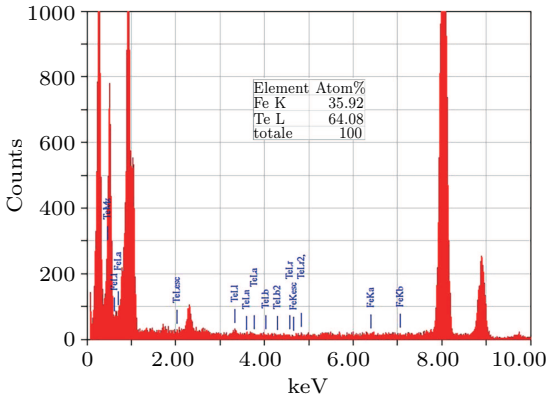


Fig. A2. EDX spectrum of the as-prepared $FeTe_2$ NCs.

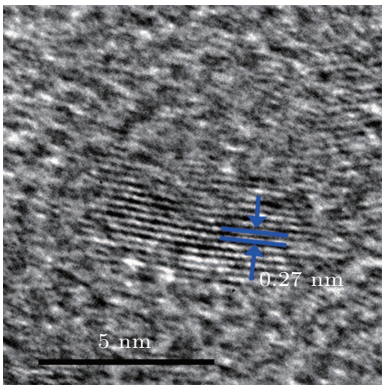


Fig. A3. HRTEM image of the as-prepared $FeTe_2$ NCs.

References

[1] Venkatasubramanian R, Colpitts T, Watko E, Lamvik M and El-Masry N 1997 *J. Cryst. Growth* **170** 817

[2] Mamur H, Bhuiyan M R A, Korkmaz F and Nil M 2018 *Renewable Sustainable Energy Rev.* **82** 4159

[3] Friederichs G M, Wörsching M P B and Johrendt D 2015 *Supercond. Sci. Technol.* **28** 095005

[4] Mal J, Nancharaiah Y V, van Hullebusch E D and Lens P N L 2016 *RSC Adv.* **6** 41477

[5] Zheng Y, Gao S and Ying J Y 2007 *Adv. Mater.* **19** 376

[6] Harrache Y and Bouarissa N 2019 *Solid State Commun.* **295** 26

[7] Ghosh A and Thangavel R 2017 *Indian J. Phys.* **91** 1339

[8] Fang L, Chen J, Xu L, Su W N, Yu Y, Xu J and Ma Z Y 2013 *Chin. Phys. B* **22** 098802

[9] Li Y, Chen J, Han X, Li Y, Zhang Z and Ma Y 2019 *Nano* **13** 1850146

[10] Liu N, Li S X, Ye Y C and Yao Y L 2018 *Chin. Phys. B* **27** 127303

[11] Tan C, Qi X, Liu Z, Zhao F, Li H, Huang X, Shi L, Zheng B, Zhang X, Xie L, Tang Z, Huang W and Zhang H 2015 *J. Am. Chem. Soc.* **137** 1565

[12] Mao Y, Kanungo M, Hemraj-Benny T and Wong S S 2006 *J. Phys. Chem. B* **110** 702

[13] Wang Y, Dai Q, Zou B, Yu W W, Liu B and Zou G 2010 *Langmuir* **26** 19129

[14] Zhu Z P, Wei B, Zhang J H and Wang J 2014 *Chin. Phys. B* **23** 077202

[15] Chen Z and O'Brien S 2008 *ACS Nano* **2** 1219

[16] Talapin D V 2008 *ACS Nano* **2** 1097

[17] Mueggenburg K E, Lin X M, Goldsmith R H and Jaeger H M 2007 *Nat. Mater.* **6** 656

[18] Nykypanchuk D, Maye M M, van der Lelie D and Gang O 2008 *Nature* **451** 549

[19] Landman U and Luedtke W D 2004 *Faraday Discuss.* **125** 1

[20] Talapin D V, Shevchenko E V, Murray C B, Titov A V and Kral P 2007 *Nano Lett.* **7** 1213

[21] Shevchenko E V, Talapin D V, Kotov N A, O'Brien S and Murray C B 2006 *Nature* **439** 55

[22] Ziherl P and Kamien R D 2001 *J. Phys. Chem. B* **105** 10147

[23] Prasad B L V, Stoeva S I, Sorensen C M and Klabunde K J 2002 *Langmuir* **18** 7515

[24] Gao J, Zhang B, Zhang X and Xu B 2006 *Angew Chem. Int. Ed. Engl.* **45** 1220

[25] Yang X, Wang Y, Sui Y, Huang X, Cui T, Wang C, Liu B, Zou G and Zou B 2012 *Langmuir* **28** 17811

[26] Wang Y, Dai Q, Wang L, Zou B, Cui T, Liu B, Yu W W, Hu M Z and Zou G 2010 *J. Phys. Chem. C* **114** 11425

[27] Yang X, Zhou B, Liu C, Sui Y, Xiao G, Wei Y, Wang X and Zou B 2017 *Nano Res.* **10** 2311

[28] Deng L, Zhao Y, Zhou P, Xu H and Wang Y 2016 *Chin. Phys. B* **25** 128704

[29] Tripp S L, Dunin-Borkowski R E and Wei A 2003 *Angew Chem. Int. Ed. Engl.* **42** 5591

[30] Tripp S L, Pusztay S V, Ribbe A E and Wei A 2002 *J. Am. Chem. Soc.* **124** 7914

[31] Wu M, Wang Y, Wang H, Wang H, Sui Y, Du F, Yang X and Zou B 2018 *Nanoscale* **10** 21928

[32] Zhang W, Yang Z, Zhan J, Yang L, Yu W, Zhou G and Qian Y 2001 *Mater. Lett.* **47** 367

[33] Liu A, Chen X, Zhang Z, Jiang Y and Shi C 2006 *Solid State Commun.* **138** 538

[34] Oyler K D, Ke X, Sines I T, Schiffer P and Schaak R E 2009 *Chem. Mater.* **21** 3655

[35] Deng D W, Li P and Gu Y Q 2009 *Cryst. Res. Technol.* **44** 629

[36] Wan B, Hu C, Feng B, Xi Y and He X 2009 *Mater. Sci. Eng. B* **163** 57

[37] Jiang P, Zhu D L, Zhu C N, Zhang Z L, Zhang G J and Pang D W 2015 *Nanoscale* **7** 19310

[38] Sines I T, Vaughn D D, Biacchi A J, Kingsley C E, Popczun E J and Schaak R E 2012 *Chem. Mater.* **24** 3088

[39] Witt E, Witt F, Trautwein N, Fenske D, Neumann J, Borchert H, Parisi J and Kolny-Olesiak J 2012 *Phys. Chem. Chem. Phys.* **14** 11706